ACS OMEGA

Open Access

http://pubs.acs.org/journal/acsodf

Article

Research on the Performance of Cement-Based Composite Borehole Sealing Material Based on Orthogonal Test

Shuqi Xu, Shanyang Wei,* Hongfei Xie, Yuzhu Liang, Xuzheng Zhu, Weidong Luo, and Fuzhi Zhu

Cite This: *ACS Omega* 2024, 9, 10799−10811

Read Online

ACCESS | Metrics & More | Article Recommendations

ABSTRACT: In order to achieve better sealing of boreholes, the performance of sealing materials is modified to improve the efficiency of coalbed methane extraction. In this paper, a new type of cement-based hole sealing material was prepared by using silicate cement (PC) and cement sulfoaluminate (SAC) as raw materials, supplemented with various additives, such as fly ash, Na_2SO_4, $Ca(OH)_2$, and poly(vinyl alcohol) (PVA) fiber. The effects of these additives on the fluidity, setting time, and compressive strength of the PC-SAC compounded cementitious pore sealing material were investigated by orthogonal tests, and the hydration process and hydration products were analyzed by X-ray diffraction (XRD), thermogravimetry-differential thermogravimetry (TG-DTG), and scanning electron microscopy (SEM). The results show that the water−cement ratio has the most significant influence on the various properties of the material; the two additives of Na_2SO_4 and $Ca(OH)_2$ play a key role in the setting time of the material; the optimal group, i.e., water−cement ratio of 0.5, fly ash of 5%, Na_2SO_4 of 1%, $Ca(OH)_2$ of 0.75%, and PVA fibers of 0.8%, is obtained by the orthogonal test method, which is the closest to the actual needs of the project. The hydration products of the optimized materials have obvious changes, and the needle-like AFt and C−S−H increase so that the performance of the materials has been significantly improved.

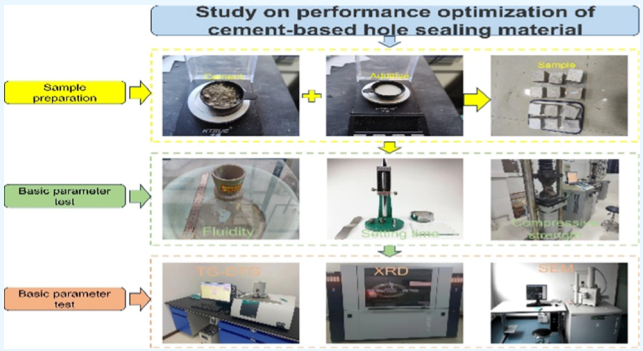

1. INTRODUCTION

Coalbed methane (CBM) is a type of unconventional natural gas that is primarily found in coal seams and the rocks surrounding them. It is a clean and efficient energy source.[1] China possesses enormous deposits of CBM, making it a significant renewable energy source in contemporary society. However, it also poses a safety risk within coal mines. Extracting CBM can significantly decrease the direct release of gas, resulting in a reduction in coal mine gas disaster accidents and an improvement in energy utilization efficiency.[2−4] Currently, the extraction efficiency of coalbed methane in China's coal mines is suboptimal. Therefore, it is imperative to implement measures aimed at enhancing the extraction efficiency of coalbed methane in order to guarantee the safe operation of coal mines. There are two primary approaches to enhance the extraction efficiency of CBM: (1) addressing the issues of low permeability, small pore size, and excessive adsorption in coal beds by employing hydraulic fracturing and water injection in coal beds.[5−7] (2) Drilling can create air leakage channels, but the application of hole sealing materials can reduce these channels and improve the efficiency of extracting CBM.[8−10] Focusing on the process of coal seam roadway mining damage, the researchers analyzed the factors affecting gas leakage during the extraction process and found a reasonable sealing hole grouting depth and grouting parameters through simulation. In addition, Fourier transform infrared spectroscopy (FTIR) and Raman spectroscopy were used to analyze the microstructure of the coal body, and combined with impact dynamics experiments to analyze the energy accumulation and energy dissipation in the rupture process of gas-containing coal. And on this basis, methods such as hydraulic fracturing coalbed water injection were improved so as to improve the extraction efficiency of coalbed methane.[5,7,11−15] The first method has been widely used, with the increasing depth of coal mining, the underground environment is more and more complex, the performance of the commonly used sealing materials can not meet the needs of the project site. Especially for the "three soft" coal seams and other special coal seams, the long condensation time and the insufficient strength of the material are easy to cause problems such as collapse in the extraction process.[16−18] Finding a way to enhance the rapid solidification properties of the hole sealing material has emerged as a pressing issue.[19−21] Fly ash and poly(vinyl alcohol) (PVA)

Received: December 7, 2023
Revised: February 1, 2024
Accepted: February 9, 2024
Published: February 22, 2024

fibers are commonly employed in cementitious materials. Fly ash is a byproduct of thermal power generation, and excessive accumulation of fly ash can have detrimental effects on the environment. By utilizing a portion of the fly ash to substitute for silicate cement, not only can the material's performance be enhanced but also waste resources can be recycled.[22−25] The addition of a significant quantity of fly ash and PVA fibers to engineered cementitious composites (ECCs) and ultrahigh-performance fiber-reinforced cementitious composites (UHTCCs) enhances the strength and tensile strain characteristics of cementitious materials. Moreover, increasing the amount of fly ash doping results in a denser distribution of cracks in the cementitious materials, leading to improved durability.[26−29] Optimal exploitation of fly ash can enhance the mechanical qualities and durability of cementitious materials, particularly the strength during the later stages. At room temperature, the activity of fly ash is minimal. To address the issue of low early strength in the fly ash-cement system, alkali exciters can be added to the material. By using strong alkali, the fly ash can be activated, leading to a faster development of strength.

Currently, numerous research studies have been conducted to enhance the effectiveness of cement. However, most of these studies focus on a single type of cement combined with various additives. There is a lack of research on the modification of cement by combining different types of cement and then adding a variety of additives. Therefore, this paper utilizes a combination of PC cement and SAC cement, followed by the addition of fly ash, Na_2SO_4, $Ca(OH)_2$, and PVA fiber for modification. Modification studies focus on solidification time and compressive strength properties of materials. The composite materials were subjected to tests to evaluate their flow, setting time, and compressive strength. Additionally, the microstructure of the materials was qualitatively and quantitatively studied using X-ray diffraction (XRD), thermogravimetry-differential thermogravimetry (TG-DTG), and scanning electron microscopy (SEM) techniques. The aim of these analyses was to enhance the overall performance of the composite materials.

2. EXPERIMENTAL SECTION

2.1. Materials and Sample Preparation. In this paper, ordinary silicate cement (PO 42.5) and sulfoaluminate cement (SAC 42.5) were selected as the experimental basis. Fly ash, Na_2SO_4, $Ca(OH)_2$, and PVA fiber were chosen as the modified materials. Fly ash is the residual ash after combustion of coal ash boiler, which is an essential active additive. However, the initial activity of fly ash is too low, so the Na_2SO_4 and $Ca(OH)_2$ were used as an alkaline exciter to activate the activity of fly ash and accelerate the hydration reaction, and finally PVA fiber was used as a neutral substance, not involved in the hydration process of the reaction, which can reduce the generation of cracks in the material, to increase the compressive strength of the material. The main chemical compositions of PC, SAC, and FA are shown in Table 1. The main hydration reactions of PC and SAC main hydration reactions are shown in eqs 1−6[30−33]

$$C_3S + H \rightarrow C{-}S{-}H\ \text{gel} + (3 - n)CH \quad (1)$$

$$2C_3A + nH \rightarrow C_4AH_{13} + C_2AH_8 \quad (2)$$

$$C_2AH_{13} + 3C\overline{S}H_2 + 14H \rightarrow C_3A{\cdot}3C\overline{S}H_{32}(AFt) + CH \quad (3)$$

Table 1. Chemical Composition

oxides	PO 42.5 (wt %)	SAC 42.5 (wt %)	fly ash II
SiO_2	21.30	8.78	45.1
Al_2O_3	6.96	33.87	24.2
CaO	61.31	42.73	5.6
Fe_2O_3	3.36	2.19	0.85
MgO	2.7	2.13	2.13
SO_3	2.0	8.515	2.1
loss on ignition	1.522	0.797	4.7

$$C_4A_3\overline{S} + 2C\overline{S}H_2 + nH \rightarrow 2Al(OH)_3 + C_3A{\cdot}3C\overline{S}H_{32}(AFt) \quad (4)$$

$$C_{12}A_7 + 12C\overline{S}H_2 + nH \rightarrow 3Al(OH)_3 + 4C_3A{\cdot}3C\overline{S}H_{32}(AFt) \quad (5)$$

$$C_2S + mH \rightarrow C{-}S{-}H + Ca(OH)_2 \quad (6)$$

2.2. Orthogonal Experimental Designs. Orthogonal testing is a method of experimental design that uses several components and levels to gather comprehensive information with a reduced number of experiments, leading to substantial savings in time and expense. Therefore, this study will utilize orthogonal testing to identify the ideal proportion of cementitious materials, allowing for the selection of the most representative program from a wide range of test combinations.

The test program employed a five-factor, four-level orthogonal test architecture. Table 2 contains the test factors

Table 2. Test Factor Level Table

factor	A	B (%)	C (%)	D (%)	E (%)
1	0.55	5	0.5	0.25	0.2
2	0.5	10	1	0.5	0.4
3	0.45	15	1.5	0.75	0.6
4	0.4	20	2	1	0.8

and their corresponding levels. Based on the L_{16} (4^5) orthogonal test program and the resulting data set, orthogonal test auxiliary software was used to construct 16 sets of test combinations with different ratios. The resultant orthogonal test is displayed in Table 3. Factors A−E represent the water−cement ratio, fly ash, Na_2SO_4, $Ca(OH)_2$, and PVA fiber, respectively. These elements are known to influence the viscosity, the time it takes for the cement to start setting, the time it takes for the cement to fully set, and the strength of the cementitious materials. The concentration of additives is quantified as a proportion of the overall weight of cementitious materials.

2.3. Sample Preparation Process. The cement specimens were made in accordance with the national standard GB/T17671-1999. In this work, a blend consisting of 60% polycarbonate (PC) and 40% calcium sulfate anhydrite (SAC) was selected.[34−37] The mass of the components was measured using a beaker and a precision balance with an accuracy of 0.01, following the proportions indicated in Table 3. The additives were incorporated into the mixed cement in proportion to its overall weight. The cement and other components were meticulously blended and agitated until completely integrated. After achieving a thorough mixture, the cement and other components were poured into a mold with dimensions of 70.7 × 70.7 × 70.7 mm^3. The mold was thereafter placed in an

https://doi.org/10.1021/acsomega.3c09804
ACS Omega 2024, 9, 10799−10811

Table 3. Orthogonal Test Design Table

group number	A	B	C	D	E
1	0.55 (A_1)	5% (B_1)	0.5% (C_1)	0.25% (D_1)	0.2% (E_1)
2	0.55	10% (B_2)	1% (C_2)	0.5% (D_2)	0.4% (E_2)
3	0.55	15% (B_3)	1.5% (C_3)	0.75% (D_3)	0.6% (E_3)
4	0.55	20% (B_4)	2% (C_4)	1% (D_4)	0.8% (E_4)
5	0.5 (A_2)	5%	1%	0.75%	0.8%
6	0.5	10%	0.5%	1%	0.6%
7	0.5	15%	2%	0.25%	0.4%
8	0.5	20%	1.5%	0.5%	0.2%
9	0.45 (A_3)	5%	1.5%	1%	0.4%
10	0.45	10%	2%	0.75%	0.2%
11	0.45	15%	0.5	0.5%	0.8%
12	0.45	20%	1%	0.25%	0.6%
13	0.4 (A_4)	5%	2%	0.5%	0.6%
14	0.4	10%	1.5%	0.25%	0.8%
15	0.4	15%	1%	1%	0.2%
16	0.4	20%	0.5%	0.75%	0.4%

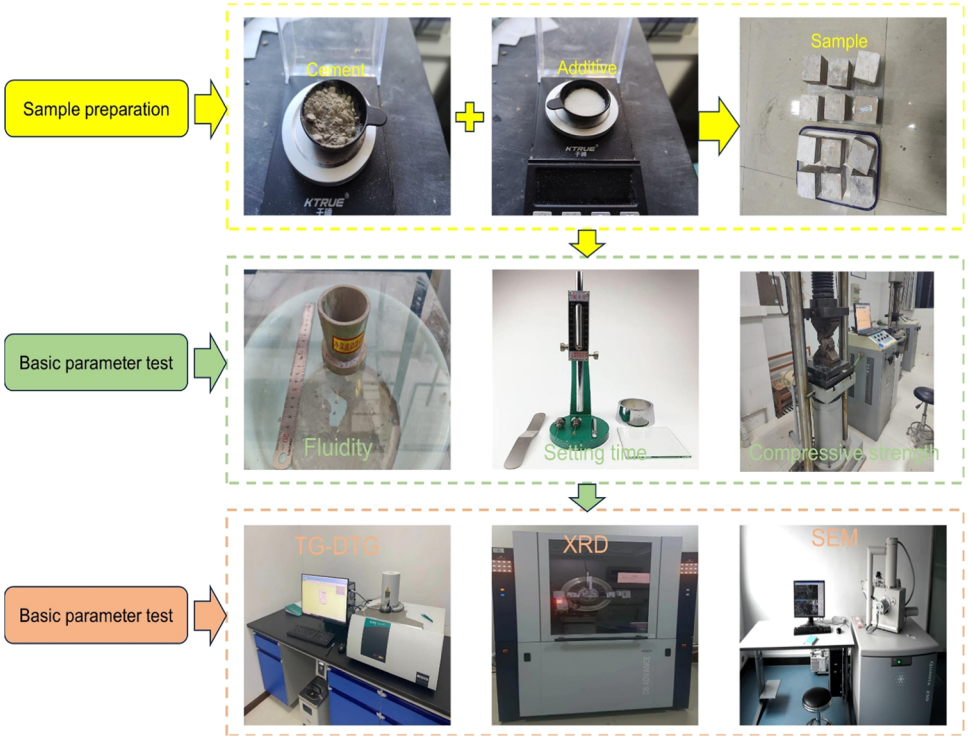

Figure 1. Experimental equipment and program.

atmosphere with a constant temperature of 20 ± 2 °C and a relative humidity of 95 °C for a period of 24 h. Subsequently, the mold was extracted and the cement was allowed to retain its initial state. The test was conducted 15 days following the maintenance. Figure 1 provides a visual representation of the precise methodology and equipment employed in the tests.

2.4. Test Methods. *2.4.1. Cementitious Sealing Material Flowability Test.* The mobility of cement mortar is tested using a truncated cone mold, as specified by the GB/T2419-94 test. Prior to the test, the necessary materials are gathered, including a sleek glass plate of 50 cm on each side, a truncated cone mold, and a steel ruler. The cement slurry is poured into the truncated cone mold and leveled. Subsequently, the truncated cone mold is promptly raised, facilitating the flow of the slurry onto the glass plate for a duration of 30 s. The extent of the slurry's dispersion is assessed by employing a steel ruler to ascertain its maximum horizontal and vertical dimensions. The experiment is replicated thrice, and the mean measurement is obtained as the fluidity of the slurry.

2.4.2. Cementitious Sealing Material Setting Time Test. The setting time of the cement was measured following the guidelines of the GB/T1346-2011 standard, using a Vickers meter. The initial test was performed 20 min following the mixing of the cement, and subsequent measurements were obtained at intervals of 5 min.

2.4.3. Uniaxial Compressive Strength Test. The YAW-3000A1 pressure testing machine, produced by Jinan Test King Group Co., Ltd., is used in the mechanical experiment to measure uniaxial compressive strength. The gadget functions using a displacement loading method and can handle a

https://doi.org/10.1021/acsomega.3c09804
ACS Omega 2024, 9, 10799−10811

maximum load capacity of 2000 kN. Every set of specimens is subjected to three tests, and the average value is regarded as the sample data. It is crucial to horizontally place the test block during the experiment to avoid the casting surface from being subjected to pressure.

2.4.4. X-ray Diffraction Analysis. The X-ray diffractometer used in this investigation is the D8 advance, produced by Bruker in Germany. The experiment utilized a sample powder consisting of particles that were 200 mesh or larger in size. Before conducting the test, the sample was dehydrated and placed in a tightly sealed bag. For every trial, 0.5 g of the specimen was incorporated. The sample must be scanned within a temperature range of 5−80 °C. The experiment should be performed utilizing a copper (Cu) target at a scanning rate of 5 °C/min.

2.4.5. Thermogravimetric Analysis. The study utilized a TG 209F3 thermal weight loss analyzer, produced by NETZSCH in Germany, to determine the kind and quantity of cement hydration reaction products by thermal weight loss analysis. After the drying process, the sample was thoroughly pulverized to obtain particles less than 80 mm in size. A 10 mg aliquot of the sample was thereafter delicately deposited into the thermal analyzer. The analyzer was filled with nitrogen (N_2) to create the internal environment. The heating rate was precisely regulated to 20 °C/min, and the temperature was carefully controlled not to exceed 1000 °C. The temperature rose at a pace of 20 °C/min.

2.4.6. SEM Analysis. The microscopic morphology of the materials was examined using a QuantuTM 250 FEG high-resolution, multipurpose scanning electron microscope manufactured by Shanghai Yuzhong Technology Company. The surface microstructure of the sealing material particles was examined utilizing the low-vacuum mode image-capturing feature of the instrument. Specimens having a radius smaller than 0.25 cm were tested by exposing them to a voltage of 20 kV. Before the test, the samples were dehydrated and kept in a Ziploc bag. In addition, a layer of gold was applied to the samples.

3. RESULTS AND DISCUSSION

3.1. Analysis of Orthogonal Test Results. The results of orthogonal experiments are presented in Table 4. The data were analyzed using polar analysis of orthogonal test to thoroughly evaluate the extent of impact of five elements, specifically water−cement ratio, fly ash, Na_2SO_4, $Ca(OH)_2$, and PVA fiber, on each characteristic of the material. In addition, the investigation sought to assess the extent of influence that each element and level had on the performance of the material.

3.1.1. Analysis of Factors Affecting Mobility. The flowability of the sealing materials was assessed and analyzed utilizing the cement flowability test technique and orthogonal test polar analysis. A numerical designation (A1−A4) was issued to each set of results, according to the water−cement ratio. *R* measured the extent of the discrepancy in the polar analysis data. Figure 2 depicts the significance of each factor's influence on the sealing materials.

The influence of each element on the flow characteristics is clearly demonstrated in Figure 2, where a reduction in the water−cement ratio leads to a proportional fall in the material's flowability. At the maximum water−cement ratio (A1), the flowability significantly exceeds the flowability characteristics of other water−cement ratios. The flowability performance decreases steadily as the amount of additional cementitious materials, especially calcium hydroxide, increases. The polar analysis results show that the water−cement ratio (RA) has a greater value than $Ca(OH)_2$ (RD), which in turn has a greater value than fly ash (RB), Na_2SO_4 (RC), and PVA (RE). More precisely, the impact of RA on the flow characteristics is considerably more pronounced in comparison to the effects of other components. In contrast, the influence of these additional parameters on the flow characteristics is rather negligible.

Table 4. Orthogonal Experimental Results

group number	fluidity/MM	initial setting time/MIN	final setting time/MIN	strength/MPa
1	158	35	55	10.47
2	155	40	62	14.76
3	151	46	70	13.91
4	148	56	81	17.32
5	126	30	57	22.35
6	118	50	75	24.94
7	125	48	70	18.56
8	133	45	60	16.27
9	98	40	60	24.45
10	103	45	59	20.57
11	93	35	58	25.86
12	102	34	56	18.90
13	88	27	49	28.16
14	83	23	50	32.86
15	75	36	56	25.65
16	89	21	53	23.80

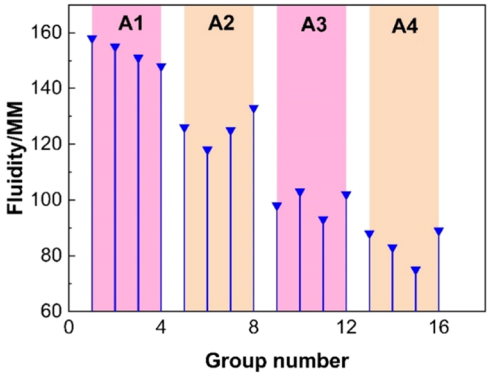

Figure 2. Variation of flow performance in orthogonal experiment.

Figure 3 shows the plot of the polar relationship between the flow properties and the factors in the orthogonal test, and the results of the polar analysis show that water−cement ratio (RA) > $Ca(OH)_2$ (RD) > fly ash (RB) > Na_2SO_4 (RC) > PVA (RE). Specifically, the influence of RA on the flow properties is significantly stronger than that of various other parameters, while the impact of these other factors on the flow properties is rather insignificant. An increase in the water−cement ratio results in a higher proportion of water in the cement paste, which promotes the suspension and dispersion of particles in the paste. For water−cement ratios over 0.5, the samples consistently exhibited excellent fluidity performance. The fluidity of the sealing material remained relatively constant, and the diffusion radius remained stable. The primary factors are as follows: An increase in the water content of the material leads to greater water absorption on the surface of the cement particles in the cement paste. Additionally, the presence of fly ash in the additive has been extensively studied and proven to cause a volcanic ash reaction when added to cement. This reaction enhances

https://doi.org/10.1021/acsomega.3c09804
ACS Omega 2024, 9, 10799−10811

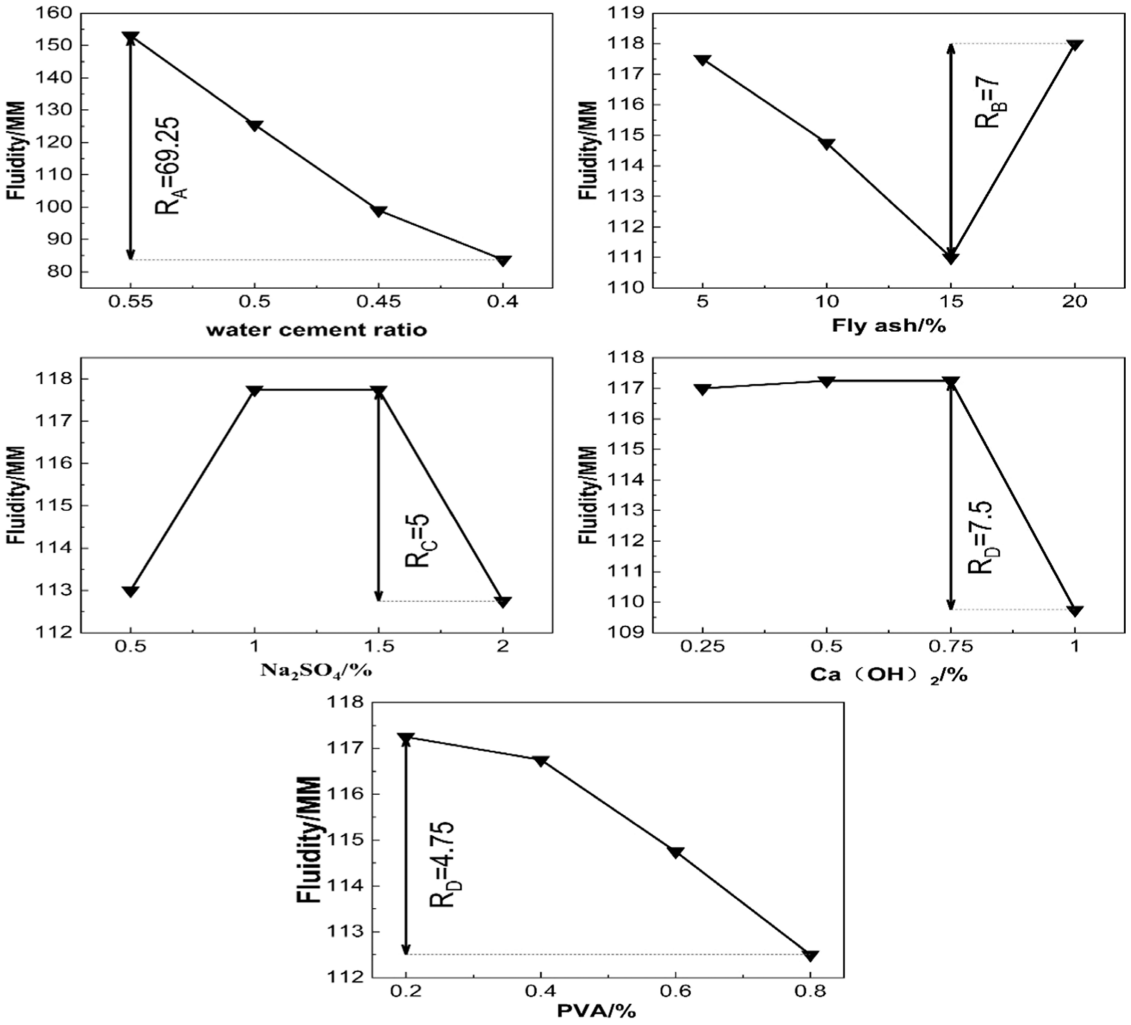

Figure 3. Relationship curve between fluidity of sealing materials and range of various factors.

hydration reactions.[38−40] Aside from the water−cement ratio, the most significant factor affecting the flow properties is $Ca(OH)_2$. This is especially true when fly ash is added in intermediate amounts. The presence of fly ash, $Ca(OH)_2$, Na_2SO_4, and other alkaline substances simultaneously enhances the activity, resulting in the production of numerous hydration products. This process consumes a substantial amount of free water and combined water, thereby reducing the fluidity of the cement slurry.[41,42] The PVA fibers are devoured by the cement slurry in a similar manner as the water content. When the PVA content exceeds 0.6%, excessive PVA causes agglomeration, resulting in uneven mixing of the cement paste and reduced fluidity. Hence, the proportion of the sealing material with appropriate fluidity is $A_1B_4C_3D_3E_1$. This means that the water−cement ratio is 0.55, the fly ash dosage is 20%, the Na_2SO_4 content is 1.5%, the $Ca(OH)_2$ content is 0.75%, and the PVA content is 1%.

3.1.2. Analysis of Factors Affecting Condensation Time. Based on the analysis of the cement setting time test method and the orthogonal test extreme difference analysis method of the sealing material flowability test results, it can be concluded that PVA fiber is a neutral substance that does not actively participate in the hydration process. Instead, PVA fibers only affect the mechanical properties of the material, such as flow properties, compressive strength, and flexural strength. Therefore, when considering the various factors that affect the setting time of the cement, PVA fibers should be excluded. The experiment utilized a composite cement consisting of 60% PC and 40% SAC. Increasing the CSA content results in a notable decrease in the setting time of the composite cement. During the hydration process, there is a struggle for effective water between SAC and PC. The hydration of PC was significantly hindered by 40% of SAC, leading to the formation of a substantial amount of calcite. This, in turn, contributed to the amplification of the delayed hydration effect.[30,43]

Based on the fluctuation of solidification time seen in the orthogonal experiments depicted in Figure 4, it can be observed that, when the water−ash ratio remains constant, the solidification time tends to increase as the catalyst content increases. An increase in the fly ash content leads to a lengthening of the solidification period. Given that the particle size of fly ash is less than the particle size of both cements, it can infiltrate the cement's pores while it is undergoing hydration, thereby reducing the contact area between the cement paste and water molecules. This results in a delay in the hydration process and an extension of the setting time. The composite material forms hydration products that envelop the cement particles. As the hydration reaction progresses, water is consistently absorbed within the cement particles, causing the proportion of unbound water in the cement slurry to increase. Consequently, the relative

https://doi.org/10.1021/acsomega.3c09804
ACS Omega 2024, 9, 10799−10811

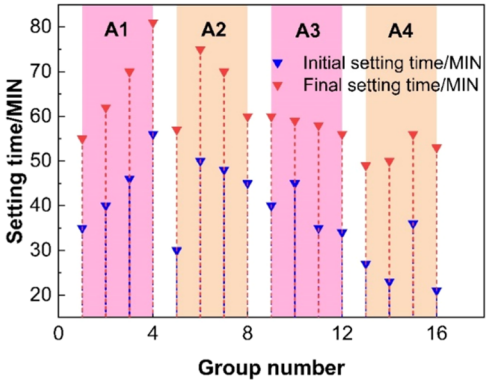

Figure 4. Variation of coagulation time in orthogonal experiment.

humidity within the slurry steadily rises. The water in the slurry undergoes diffusion and dispersion mostly due to the force of gravity, resulting in the continuous hydration of the unhydrated cement particles and the filling of the slurry's pores.

As shown in Figure 5, the curves of the relationship between the setting time of the sealing material and the polarity of each factor reveal the significance of the influence of each factor on the setting time, the significance of the factors affecting the initial setting time in the order of significance: water−cement ratio (RA) > Na_2SO_4 (RC) > $Ca(OH)_2$ (RD) > fly ash (RB), and the significance of the factors affecting the final setting time in the order of significance: water−cement ratio (RA) > $Ca(OH)_2$ (RD) > Na_2SO_4 (RC) > fly ash (RB). These findings indicate that the water−cement ratio has the most significant impact on setting time, with Na_2SO_4 and $Ca(OH)_2$ having a comparatively stronger influence. While the water−cement ratio remains the primary determinant, the decrease in water content hinders the hydration reaction, resulting in a shorter setting time. However, when it comes to the setting time, the variation in water−ash ratio and other parameters is minimal compared to the variation in fluidity. The impact of Na_2SO_4 on the initial setting time is more significant compared to $Ca(OH)_2$. The variation in factors impacting the initial and final setting is due to the shorter duration of the initial setting time and differences in the degree of hydration. As the hydration reaction progresses over time, the impact of alkaline excitation on fly ash becomes increasingly apparent. The alkalinity of $Ca(OH)_2$ is stronger than that of Na_2SO_4, resulting in a higher degree of hydration during the final coagulation stage compared to the initial coagulation stage. $Ca(OH)_2$ is more effective in stimulating the fly ash, and the volcanic ash reaction of the fly ash further enhances the hydration reaction. Hence, the composite possesses an appropriate setting time with a ratio of $A_1B_3C_4D_4$. This implies that the water−cement ratio is 0.55, the dosage of fly ash is 15%, the Na_2SO_4 content is 2%, and the $Ca(OH)_2$ content is 1%.

3.1.3. Analysis of Factors Affecting Compressive Strength. By employing the cement setting time test method and the orthogonal test extreme difference analysis method, the results of the fluidity test of the sealing material were visualized and analyzed. Figure 6 illustrates the variation in compressive strength during the orthogonal test, revealing that the A4 group exhibits significantly higher strength compared to the A1 group.

Evidently, the strength is significantly influenced by the water−cement ratio. The alteration of the water−cement ratio affects the amount of free water in the cement paste, leading to a decrease in relative humidity. Furthermore, this orthogonal experiment only requires a mere 14 days of upkeep, indicating a much reduced duration. The impact of volcanic ash, namely, fly ash, takes around 14 days to fully manifest. Initially, fly ash hinders the early strength of cement materials, but later on, it aids in boosting strength. The strength of the seventh and eighth groups declined further, while the water−cement ratio remained

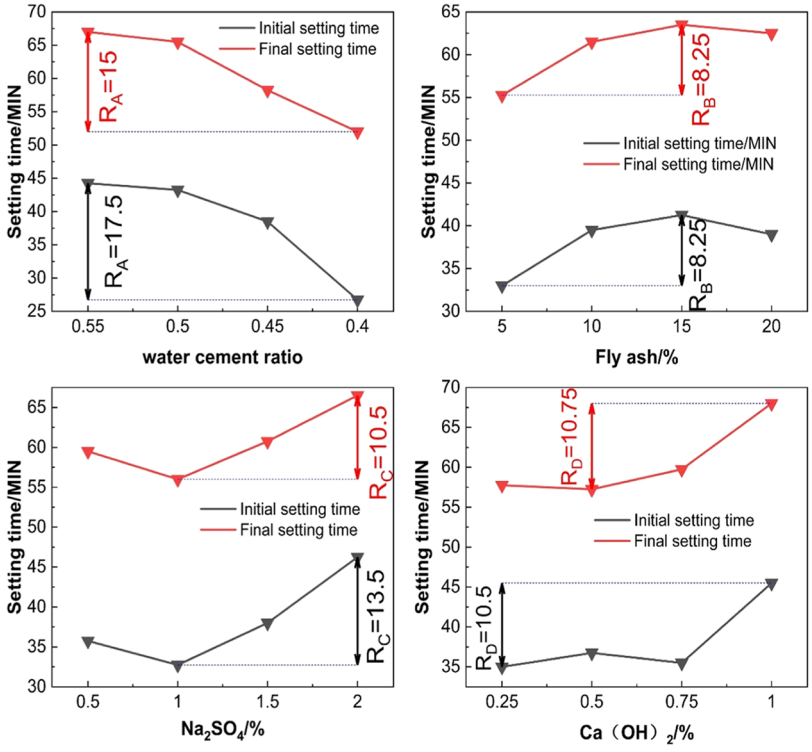

Figure 5. Relationship curve between setting time of sealing materials and range of various factors.

https://doi.org/10.1021/acsomega.3c09804
ACS Omega 2024, 9, 10799−10811

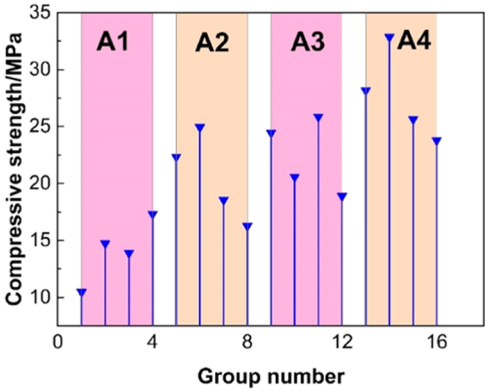

Figure 6. Changes of compressive strength in orthogonal test.

unchanged. The change in strength was more significant compared to the first two groups. The primary factor is the alteration of the composition of PVA fiber, resulting in a modification of the material's mechanical characteristics. Another factor is that $Ca(OH)_2$ and Na_2SO_4 enhance the reactivity of fly ash and expedite the hydration process, resulting in a significant formation of AFt.[44,45]

According to the extreme difference analysis in Figure 7, it can be seen that the significance of the effect of each factor on compressive strength is in the following order: water−cement ratio (RA) > PVA fiber (RE) > FA (RB) > Na_2SO_4 (RC) > $Ca(OH)_2$ (RD). The primary determinants were the ratio of water to cement and the presence of PVA fiber. The compressive strength ranged from 10.47 MPa in the first group to 32.86 MPa in the 14th group over 16 sets of testing. There was a significant amount of variety. However, when considering the same water−cement ratio, the most significant deviation should occur in the 14th and 16th groups at the A4 level. The compressive strength exhibits a disparity of 9.06, with the alkaline substance content being the lowest among the compounds in the 14th group, while the fiber content is certainly the highest. This is consistent with the findings derived from the orthogonal test. Hence, the ideal combination ratio for achieving the highest compressive strength is $A_4B_2C_1D_4E_4$ at a proportion of 0.4, together with 10% fly ash, 0.5% Na_2SO_4, 1% $Ca(OH)_2$, and 0.8% PVA. Analysis of the optimal group ratios reveals that a decrease in fly ash content enhances compressive strength, whereas the water−cement ratio and PVA fiber have a substantial positive effect. Calcium hydroxide plays a significant role in the hydration reaction of both cements, utilizing a substantial quantity of free

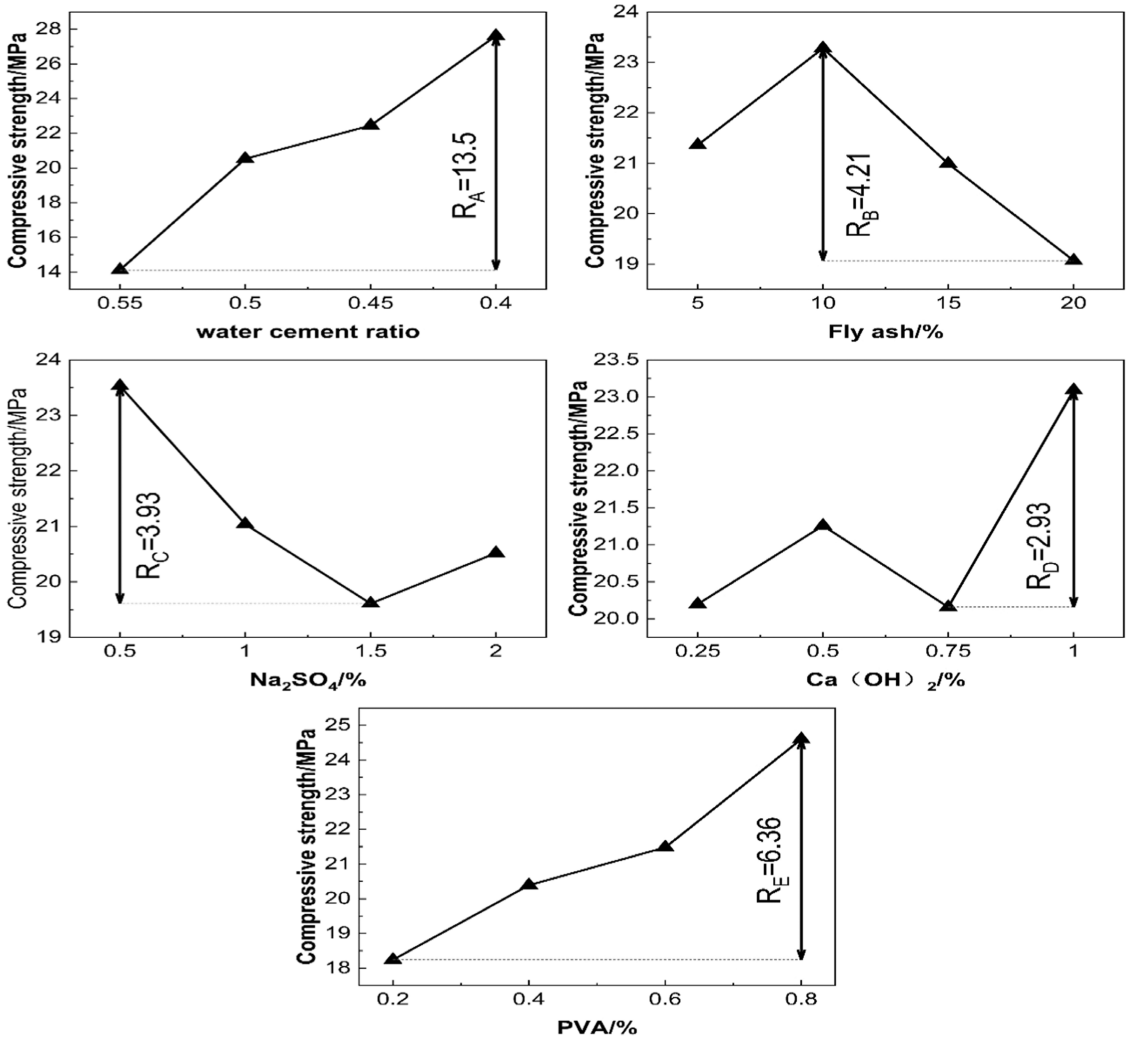

Figure 7. Relationship curve between compressive strength of sealing materials and range of various factors.

https://doi.org/10.1021/acsomega.3c09804
ACS Omega 2024, 9, 10799−10811

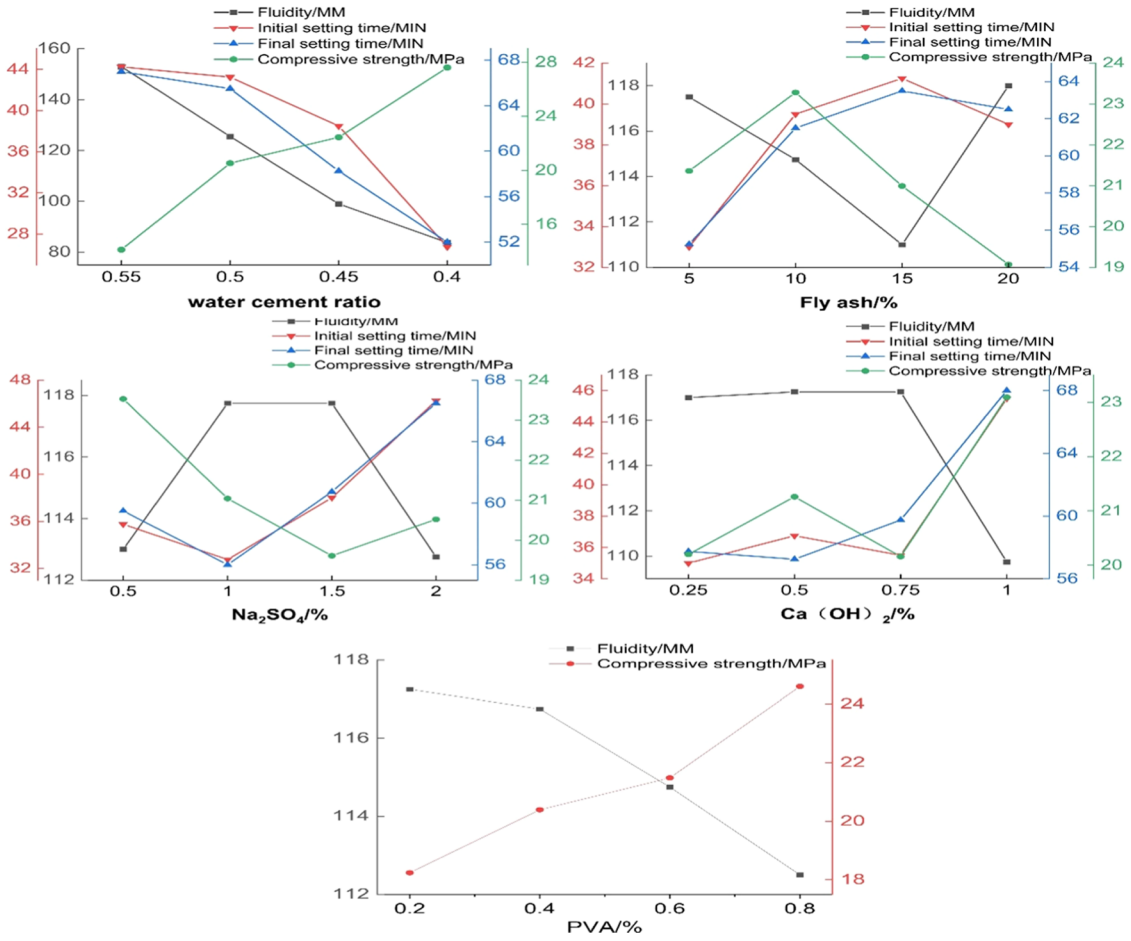

Figure 8. Comprehensive analysis diagram of orthogonal test of sealing materials.

water to produce a considerable amount of calcium alumina, hence enhancing the compressive strength.

3.1.4. Comprehensive Analysis of Orthogonal Tests. The comprehensive analysis diagram of orthogonal tests of sealing materials was used to thoroughly examine the effects of water−cement ratio, fly ash, Na_2SO_4, $Ca(OH)_2$, and PVA fiber on the initial setting time, final setting time, and compressive strength of the materials. The selection of the ideal mix of components and levels was achieved by integrating the requirements of the trial outcomes.

Figure 8a illustrates a clear correlation between the decrease in water−cement ratio and the decrease in flowability and initial and final setting times. Additionally, it shows that the compressive strength increases as the water−cement ratio decreases. The strength of the material is an important factor to consider; hence, a water−cement ratio of 0.5 is chosen.

Based on the observation of Figure 8b, it is evident that the fluidity exhibits a first increase followed by a subsequent decrease when the fly ash concentration increases. The initial and final setting time exhibits an initial increase followed by a minor decrease, while the compressive strength shows an initial increase followed by a subsequent decline. When fly ash is present in a 10% concentration, the three performance metrics show improved performance. Thus, fly ash is considered to be 10%.

As depicted in Figure 8c, the fluidity of the substance initially increases and subsequently reduces with the rise in Na_2SO_4 content. Similarly, the compressive strength experiences a decline followed by an increase. When the concentration of Na_2SO_4 increased from 0.5 to 1%, the alteration in setting time was minimal; however, the flow and compressive strength exhibited a significant variation. Thus, Na_2SO_4 is selected as 1% for thorough evaluation.

Figure 8d shows that when the $Ca(OH)_2$ content is low, it has a small impact on the flow. However, when the content exceeds 0.75%, the flow undergoes significant changes. Similarly, the compressive strength and initial setting time increase initially with the increase in $Ca(OH)_2$ content, but then decrease and eventually increase substantially. The final setting time initially decreases and then increases with the increase in $Ca(OH)_2$ content. Therefore, considering all factors, the hydrogen content should be taken into account. Hence, the concentration of calcium hydroxide was selected as 0.5% to ensure thorough evaluation.

Based on the observation of Figure 8e, it is evident that the primary impact of PVA fiber is on the flow and compressive strength. These two parameters are directly and inversely correlated with the amount of PVA fiber added. Therefore, to ensure that both indicators are at an optimal level, a comprehensive analysis suggests that the appropriate amount of PVA fiber to be used is 0.6%.

Based on the experimental data and the findings of the orthogonal test, it has been determined that the optimal group is the fifth group.

The primary objective of this study is to address the issue of excessive gas in the Guizhou region. The main focus is on

https://doi.org/10.1021/acsomega.3c09804
ACS Omega 2024, 9, 10799−10811

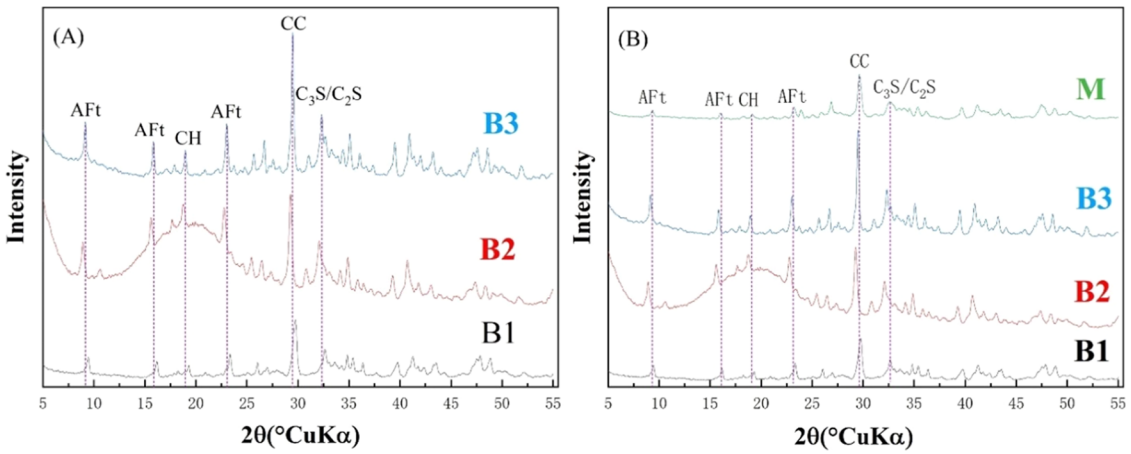

Figure 9. XRD spectrum of hydration products of sealing materials.

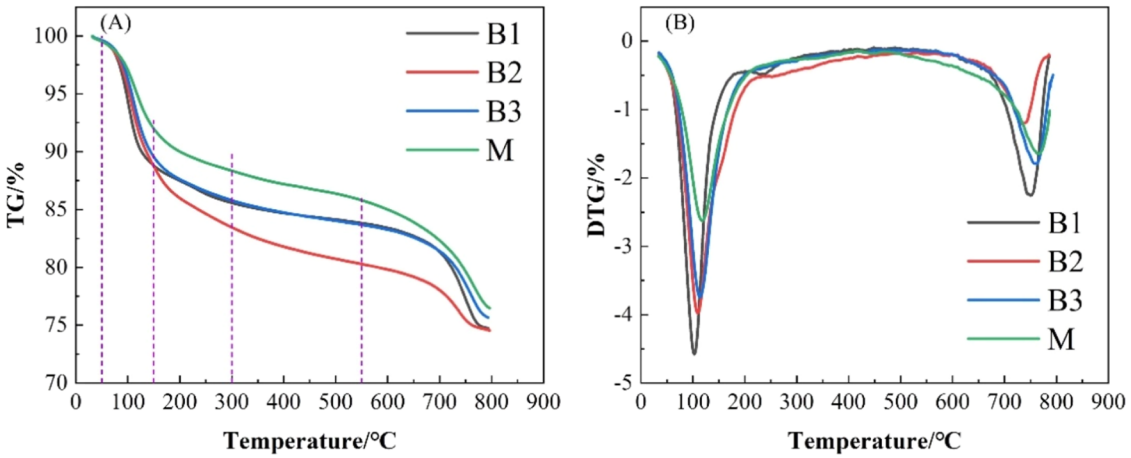

Figure 10. TG-DTG diagram of the hydration product of sealing material.

optimizing the performance of the material's setting process and retrieving data. Typically, the setting time for conventional silicate cement ranges from 45 to 390 min. However, the cement-based sealing material developed in this research controls the setting time to be within 60−120 min. This significant reduction in setting time greatly enhances the material's efficiency and operational effectiveness. Upon reviewing the relevant research, it is evident that the material's fluidity is inferior when compared to the performance described in the literature.[46,47] However, it does possess certain advantages in terms of strength and setting time.

3.2. Microstructure Analysis of Optimized Materials. Based on the analysis of 16 sets of trials, it was determined that group V was the most optimal. Compared to previous trials conducted in other groups, this group demonstrated superior flow characteristics, setting time, and compressive strength. Therefore, the 1st, 5th, and 14th groups were selected for microscopic examinations. In addition, a control group labeled as M was created, consisting of a blend of 60% PC cement and 40% SAC cement, without any further additives. The water−cement ratio was set at 0.5. The first, fifth, and 14th groups were designated as B1, B2, and B3, respectively.

3.2.1. X-ray Diffraction Analysis. Figure 9A exhibits the X-ray diffraction (XRD) spectra of the experimental groups that include supplementary additives. The spectra suggest that the main constituents of the pore sealing materials in cement are AFt, $Ca(OH)_2$, C_2S, C_3S, and $CaCO_3$. While the intensities of the diffraction peaks in the three experimental groups do not suggest the existence of any novel substances, the change is confined to the quantity of products. This is consistent with the previously documented results indicating the utilization of various additives only impacted the amount of goods, without modifying the characteristics of the products. Figure 9B clearly depicts a significant discrepancy in the quantity of products among the control blank M and the three experimental groups. This phenomenon can be explained by the rapid generation of substantial amounts of calomel after the hydration of PC- SAC blended cements. Nevertheless, the addition of alkaline admixtures did not lead to the creation of novel compounds. An examination of the alterations in cement hydration reaction materials indicated a significant augmentation in the quantity of $Ca(OH)_2$ and C_3S/C_2S products during the hydration process. Specifically, the quantity of products in group B3 showed a notable modification, suggesting that the inclusion of additives improves the process of hydration. As a result, the greater amount of cement hydration products causes an increase in the density of specimens and enhances their strength.[48] The significant increase in the amount of calomel expedited the rapid enhancement of durability in the composite cement system. Additives were employed to increase the AFt content, which in turn promoted the hydration of a particular amount of C_3S and C_2S minerals, leading to the creation of C−S−H gels and $Ca(OH)_2$ crystals. The presence of fly ash and cement contained a certain amount of silica; however, the addition of

https://doi.org/10.1021/acsomega.3c09804
ACS Omega 2024, 9, 10799−10811

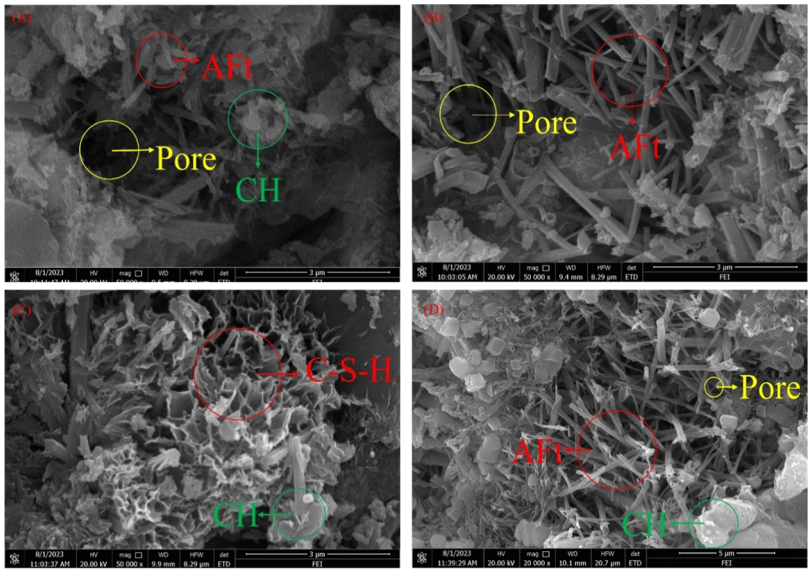

Figure 11. Microstructure diagram of sealing material.

admixtures reduced the silica content and resulted in the formation of C−S−H gels. Later, large amounts of C−S−H gels were coated on the surfaces of various materials.

3.2.2. Thermogravimetric Analysis. Thermogravimetric analysis is commonly employed alongside XRD analysis to get significant insights into the mechanisms occurring during the hydration process and the formation of noncrystalline X-ray phases. Upon analyzing the TG curves illustrated in Figure 10A, it is apparent that the curve representing the control group M is situated at a lower location compared to the curves of the other three groups. This observation indicates that the hydration process in the experimental group, which involves the admixture, takes place at a faster pace in comparison to the control group. Once again, it has been proven that the incorporation of additives improves the process of hydration reaction. The thermogravimetric (TG) curves display a primary mass reduction that may be classified into two clearly defined stages.

(I) Stage I: The cement paste had a significant reduction in weight within the temperature range of 50−150 °C. The main component that caused the decrease in bulk during this stage was the desiccation of calomel. Furthermore, it was confirmed that the main products generated during the initial process of hydration consisted mostly of calomel.[49,50] Among the three experimental groups, the 14th group experienced the lowest degree of mass reduction, whereas the first and fifth groups displayed identical degrees of mass loss. The steeper incline of the TG curve between 50 and 150 °C suggests that the fifth group undergoes a more rapid decrease in mass compared to the other two groups. After examining the concentrations of Na_2SO_4 and $Ca(OH)_2$ in the three experimental groups, it is clear that the fifth group has larger quantities of these compounds in comparison to the other two groups. This discovery indicates that the interaction between the two alkaline additives improves the hydration process in the fifth group, exceeding the hydration levels of the other groups.

(II) Stage II: There was a reduction in the weight of the cement paste when exposed to temperatures ranging from 300 to 550 °C. The main factor responsible for this step was the dehydration and decomposition of $Ca(OH)_2$. Furthermore, it is important to mention that the cement used in this case was not pure silicate cement, but rather a composite cement composed of PC-SAC. At this level, the SAC content is 40%. The combination of SAC results in the generation of a substantial quantity of calcium alumina during the process of hydration. The presence of calcium alumina obstructs the required water absorption for the hydration of PC and decelerates the hydration process. Currently, the fifth group still has the largest rate of mass loss. The key difference is that the 14th group experiences a lower level of mass reduction compared to the first group within the temperature range of 50−150 °C. Nevertheless, once the temperature reaches 300−550 °C, the 14th group ultimately exceeds the first group in terms of the amount of mass lost. The changes that occur during this stage mostly result from the impact of fly ash. Fly ash has a negligible effect on the initial hydration process. As the stage advances, the impact of fly ash gradually decreases. Nevertheless, the existence of fly ash amplifies the formation of calcite and $Ca(OH)_2$ in group XIV, leading to heightened mass reduction during this phase.

3.2.3. SEM Analysis. Additives have the ability to enhance the overall mechanical properties of cementitious materials by improving their microscopic structure. Figure 11 exhibits the microscopic features of cementitious materials used for sealing pores. Figure 11A depicts the microstructure of the control group M, Figure 11B depicts the microstructure of B1, Figure 11C depicts the microstructure of B2, and Figure 11D depicts the microstructure of group B3. Some of the main hydration products AFt, CH, and C−S−H gels can be seen in Figure 11. Among them, calcite is widely distributed in the hydration products and interspersed with each other. From Figure 11A, it can be clearly observed that the hydration products of control M are less, only a few needle-like AFt crystals and massive CH can be observed, and the pores are larger. In Figure 11B, it can be seen that a significant improvement occurs after the addition of additives, with a significant increase in the number of AFt crystals of hydration products and a reduction in the pore space. This indicates that when the cementitious materials are doped with additives, the hydration reaction is accelerated and more AFt and CH are generated, which also makes the microstructure of the materials denser and improves the previous microstructure. From Figure 11C,D, it is more obvious that there are more needle-like Aft and lamellar CH crystals, especially the number of Aft has changed significantly. This change can be

https://doi.org/10.1021/acsomega.3c09804
ACS Omega 2024, 9, 10799−10811

viewed from the macroscopic angle and microscopic roles, from the macroscopic angle is mainly reflected in the increase of compressive strength, more hydration products such as AFt, CH, and C−S−H gel make the material stronger, and from the microscopic angle, more hydration products such as Aft and CH can be seen, and the pores are more densely packed. Figure 11C shows a more obvious reticulate C−S−H gel structure, like a film covering the surface of the cement paste, reticulate and lamellar C−S−H gel with stronger cementing ability and larger specific surface area filling the pores in three-dimensional space, like a skeleton connecting the hydration products such as AFt, CH, etc. so that the cementitious composites have a certain degree of strength.[50,51]

4. CONCLUSIONS

The study focused on the development of a novel cement-based pore sealing material. The proportions of each component were determined by an orthogonal test. The microstructure of the pore sealing material was analyzed using XRD, TG-DTG, and SEM. The primary research findings are as follows:

(1) Based on the findings of the orthogonal test, the water−cement ratio has the most significant impact on the material's various qualities, particularly on its flow properties. The influence of the water−cement ratio on the flow properties is of utmost importance. Fly ash and $Ca(OH)_2$ have the second highest impact on flowability performance. In terms of setting time, $Ca(OH)_2$ has a stronger influence among the two alkaline additives, since it effectively enhances the hydration reaction. PVA fiber has a significant impact on compressive strength, effectively enhancing the material's compressive strength.

(2) At present, the commonly used sealing material is pure silicate cement, and when the water−cement ratio is 0.5, the setting time is 174 min, and the strength is 18 MPa, while the optimized optimal group of sealing material shortens the setting time to less than 60 min, which is 34.48% higher. The compressive strength is 22 MPa, an increase of 22.22%. The new material performance focuses on optimizing the setting time and compressive strength.

(3) Based on a comparison with existing technical indicators, the materials investigated in this study exhibit significant performance advantages, particularly in terms of condensation time. While typical materials require 39−450 min for condensation, the materials studied in this paper achieve condensation within 120 min, resulting in a substantial reduction in condensation time.

(4) The microscopic test findings indicate that the optimized pore sealing material, when exposed to additives, exhibited an increase in the quantity of hydration products, including a significant presence of needle-shaped AFt and CH crystals. The PVA fibers served as the framework for the hydration products in the microstructure analysis, effectively occupying the pores in the three-dimensional space, resulting in a substantial enhancement in material strength.

■ ASSOCIATED CONTENT

Data Availability Statement

Data will be made available upon request.

■ AUTHOR INFORMATION

Corresponding Author

Shanyang Wei − *Mining College of Guizhou University, Guiyang, Guizhou 550025, China;* orcid.org/0000-0001-7293-1072; Email: sywei1@gzu.edu.cn

Authors

Shuqi Xu − *Mining College of Guizhou University, Guiyang, Guizhou 550025, China*

Hongfei Xie − *Science and Technology Innovation Department of Guizhou Energy Group, Guiyang, Guizhou 550081, China*

Yuzhu Liang − *Science and Technology Innovation Department of Guizhou Energy Group, Guiyang, Guizhou 550081, China*

Xuzheng Zhu − *Mining College of Guizhou University, Guiyang, Guizhou 550025, China*

Weidong Luo − *Guizhou Energy Group Research Institute Co., Ltd., Guiyang, Guizhou 550025, China*

Fuzhi Zhu − *Guizhou Energy Group Research Institute Co., Ltd., Guiyang, Guizhou 550025, China*

Complete contact information is available at: https://pubs.acs.org/10.1021/acsomega.3c09804

Author Contributions

S.X.: investigation, data curation, methodology, writing—original draft. Wei Shanyang: supervision, conceptualization, funding acquisition, review and editing. H.X.: sources, project administration, funding acquisition, supervision. Y.L.: investigation. Shilang. X.Z.: software, review and editing. W.L.: writing—review and editing. Zhu Fuzhi: visualization, investigation.

Notes

The authors declare no competing financial interest.

■ ACKNOWLEDGMENTS

This work was financially supported by the Guizhou Provincial Key Technology R&D Program (No. [2021] General Projects 353 & No. [2021] General Projects 514) and Guizhou Provincial Central Guiding Locality Science and Technology Development Fund Project (Qianke Central Guiding Locality No. [2021] 4005).

■ REFERENCES

(1) Li, X.; Chen, S.; Wang, S.; et al. Study on in situ stress distribution law of the deep mine: taking Linyi mining area as an example. *Adv. Mater. Sci. Eng.* **2021**, *2021*, 1−11.

(2) Wang, K.; Du, F. Coal-gas compound dynamic disasters in China: a review. *Process Saf. Environ. Prot.* **2020**, *133*, 1−17.

(3) Li, B.; Zhang, J.; Ding, Z.; et al. A dynamic evolution model of coal permeability during enhanced coalbed methane recovery by N 2 injection: experimental observations and numerical simulation. *RSC Adv.* **2021**, *11* (28), 17249−17258.

(4) Kremieniewski, M.; Wiśniowski, R.; Stryczek, S.; Orłowicz, G. Possibilities of limiting migration of natural gas in boreholes in the context of laboratory studies. *Energies* **2021**, *14* (14), 4251.

(5) Wang, G.; Wang, E.; Huang, Q.; Li, S. Effects of cationic and anionic surfactants on long flame coal seam water injection. *Fuel* **2022**, *309*, No. 122233.

(6) Shreiber, A.; Portnikov, D.; Kalman, H. Theoretical and experimental analyses of energy distribution between particle and contact surface under static and dynamic loads. *Powder Technol.* **2021**, *380*, 358−367.

(7) Pang, Y.; Wang, G.; Ding, Z. Mechanical model of water inrush from coal seam floor based on triaxial seepage experiments. *Int. J. Coal Sci. Technol.* **2014**, *1*, 428−433.

https://doi.org/10.1021/acsomega.3c09804
ACS Omega 2024, 9, 10799−10811

(8) Zhang, J.; Li, G.; Yang, X.; et al. Study on a high strength ternary blend containing calcium sulfoaluminate cement/calcium aluminate cement/ordinary Portland cement. *Constr. Build. Mater.* **2018**, *191*, 544−553.
(9) Sitarz, M.; Urban, M.; Hager, I. Rheology and Mechanical Properties of Fly Ash-Based Geopolymer Mortars with Ground Granulated Blast Furnace Slag Addition. *Energies* **2020**, *13* (10), 2639.
(10) Kremieniewski, M. Influence of Hblock Fine-Grained Material on Selected Parameters of Cement Slurry. *Energies* **2022**, *15* (8), 2768.
(11) Wang, K.; Dong, H.; Guo, Y.; et al. Gas drainage performance evaluation in coal under non-uniform stress with different moisture content: Analysis, simulation and field verification. *Fuel* **2021**, *305*, No. 121489.
(12) Liu, X.; Jia, X.; Niu, Y.; et al. Alterations in coal mechanical properties and permeability influenced by liquid CO_2 phase change fracturing. *Fuel* **2023**, *354*, No. 129254.
(13) Nie, B.; Liu, X.; Yang, L.; et al. Pore structure characterization of different rank coals using gas adsorption and scanning electron microscopy. *Fuel* **2015**, *158*, 908−917.
(14) Kong, X.; He, D.; Liu, X.; et al. Strain characteristics and energy dissipation laws of gas-bearing coal during impact fracture process. *Energy* **2022**, *242*, No. 123028.
(15) He, X.; Liu, X.; Nie, B.; Song, D. FTIR and Raman spectroscopy characterization of functional groups in various rank coals. *Fuel* **2017**, *206*, 555−563.
(16) He, S.; Ou, S.; Lu, Y.; et al. Failure mechanism of methane drainage borehole in soft coal seams: Insights from simulation, theoretical analysis and in-borehole imaging. *Process Saf. Environ. Prot.* **2022**, *168*, 410−421.
(17) Zhang, Q.; Liu, Q.; Lou, Y.; Kong, D. Deviation principles of gas drainage drilling in three-soft outburst coal seams. *Geotech. Geol. Eng.* **2022**, *40* (6), 3147−3168.
(18) Qiu, D.; Wu, Y.; Li, L. Evaluation of the Gas Drainage Effect in Deep Loose Coal Seams Based on the Cloud Model. *Sustainability* **2022**, *14* (19), 12418.
(19) Sun, Z.; Li, X.; Wang, K.; et al. Determination of key technical parameters in the study of new pressure sealing technology for coal seam gas extraction. *Int. J. Environ. Res. Public Health* **2022**, *19* (9), 4968.
(20) Wu, H.; Li, X.; Gao, X.; et al. Development and application of water sealing technology for gas drainage boreholes. *ACS Omega* **2022**, *7* (1), 733−743.
(21) Xiong, W. Comparative analysis of sealing effect of different hole sealing processes in coal mine. *J. Phys.: Conf. Ser.* **2021**, *2005* (1), No. 012205.
(22) Das, D.; Rout, P. K. A Review of Coal Fly Ash Utilization to Save the Environment. *Water, Air, Soil Pollut.* **2023**, *234* (2), No. 128.
(23) Chen, F.; Zhang, Y.; Liu, J.; et al. Fly ash based lightweight wall materials incorporating expanded perlite/SiO_2 aerogel composite: Towards low thermal conductivity. *Constr. Build. Mater.* **2020**, *249*, No. 118728.
(24) Debnath, K.; Das, D.; Rout, P. K. Effect of mechanical milling of fly ash powder on compressive strength of geopolymer. *Mater. Today: Proc.* **2022**, *68*, 242−249.
(25) Das, D.; Rout, P. K. Synthesis and characterization of fly ash and GBFS based geopolymer material. *Biointerface Res. Appl. Chem.* **2021**, *11* (6), 14506−14519.
(26) Li, Q.; Huang, B.; Xu, S.; et al. Compressive fatigue damage and failure mechanism of fiber reinforced cementitious material with high ductility. *Cem. Concr. Res.* **2016**, *90*, 174−183.
(27) Yu, J.; Lin, J.; Zhang, Z.; Li, V. C. Mechanical performance of ECC with high-volume fly ash after sub-elevated temperatures. *Constr. Build. Mater.* **2015**, *99*, 82−89.
(28) Shoji, D.; He, Z.; Zhang, D.; Li, V. C. The greening of engineered cementitious composites (ECC): A review. *Constr. Build. Mater.* **2022**, *327*, No. 126701.
(29) Fu, X.; Yang, C.; Liu, Z.; et al. Studies on effects of activators on properties and mechanism of hydration of sulphoaluminate cement. *Cem. Concr. Res.* **2003**, *33* (3), 317−324.
(30) Xu, Y.; He, T.; Ma, X.; Luo, R. The influence of calcium sulphoaluminate cement on the hydration process of cement paste mixed with alkali free liquid accelerator. *Mater. Today Commun.* **2022**, *33*, No. 104622.
(31) Bullard, J. W.; Jennings, H. M.; Livingston, R. A.; et al. Mechanisms of cement hydration. *Cem. Concr. Res.* **2011**, *41* (12), 1208−1223.
(32) Lu, Z.; Kong, X.; Jansen, D.; et al. Towards a further understanding of cement hydration in the presence of triethanolamine. *Cem. Concr. Res.* **2020**, *132*, No. 106041.
(33) Zhang, Z.; Qian, S.; Ma, H. Investigating mechanical properties and self-healing behavior of micro-cracked ECC with different volume of fly ash. *Constr. Build. Mater.* **2014**, *52*, 17−23.
(34) Huang, G.; Pudasainee, D.; Gupta, R.; Liu, W. V. Extending blending proportions of ordinary Portland cement and calcium sulfoaluminate cement blends: Its effects on setting, workability, and strength development. *Front. Struct. Civ. Eng.* **2021**, *15*, 1249−1260.
(35) Yang, S.; Li, G.; Zhang, G. The Effect of CH on Improving the Carbonation Resistance of OPC-CSA Binary Blends. *Materials* **2023**, *16* (9), 3595.
(36) Wolf, J. J.; Jansen, D.; Goetz-Neunhoeffer, F.; Neubauer, J. Impact of varying Li_2CO_3 additions on the hydration of ternary CSA-OPC-anhydrite mixes. *Cem. Concr. Res.* **2020**, *131*, No. 106015.
(37) Kothari, A.; Tole, I.; Hedlund, H.; et al. Partial replacement of OPC with CSA cements−effects on hydration, fresh and hardened properties. *Adv. Cem. Res.* **2023**, *35* (5), 207−224.
(38) Nar, M.; Karpuzcu, M.; Anakc, H. Effect of Waste Marble Powder and Fly Ash on the Rheological Characteristics of Cement Based Grout. *Civ. Eng. J.* **2019**, *5* (4), 777−788.
(39) Tkaczewska, E. Effect of size fraction and glass structure of siliceous fly ashes on fly ash cement hydration. *J. Ind. Eng. Chem.* **2014**, *20* (1), 315−321.
(40) Han, F.; Zhang, Z.; Liu, J.; Yan, P. Hydration kinetics of composite binder containing fly ash at different temperatures. *J. Therm. Anal. Calorim.* **2016**, *124*, 1691−1703.
(41) Cui, Y.; Liu, J.; Wang, L.; et al. Effect of fly ash with different particle size distributions on the properties and microstructure of concrete. *J. Mater. Eng. Perform.* **2020**, *29*, 6631−6639.
(42) Hu, Y.; Xie, W.; Zou, F.; et al. Study on Mechanical and Microscopic Properties of Fly Ash Cement-Based Materials in High Geothermal Environment. *Adv. Civ. Eng.* **2022**, *2022*, No. 1768562.
(43) Donatello, S.; Fernández-Jimenez, A.; Palomo, A. Very high volume fly ash cements. Early age hydration study using Na_2SO_4 as an activator. *J. Am. Ceram. Soc.* **2013**, *96* (3), 900−906.
(44) Wang, J.; Wang, Y.; Yu, J.; et al. Effects of sodium sulfate and potassium sulfate on the properties of calcium sulfoaluminate (CSA) cement based grouting materials. *Constr. Build. Mater.* **2022**, *353*, No. 129045.
(45) Hao, M.; Song, X.; Shi, H.; et al. Experimental investigation of cement-based sealing materials for degasification using coal-bed methane drainage system. *Mater. Exp.* **2018**, *8* (2), 113−122.
(46) Zhou, A.; Wang, K. A new inorganic sealing material used for gas extraction borehole. *Inorg. Chem. Commun.* **2019**, *102*, 75−82.
(47) Lian, H.; Yi, H.; Dai, Z.; et al. Experimental Investigation on the Mixture Ratio and Diffusion Performance of Grouting Materials for Water Bursting Prevention in Coal Mines. *Adv. Mater. Sci. Eng.* **2021**, *2021*, 1−11.
(48) Zhang, J.; Li, B.; Wang, B.; et al. Preparation and Performance Investigation of Optimized Cement-Based Sealing Materials Based on the Response Surface Methodology. *ACS Omega* **2022**, *7* (29), 25380−25393.
(49) Salvador, R. P.; Rambo, D. A. S.; Bueno, R. M.; et al. On the use of blast-furnace slag in sprayed concrete applications. *Constr. Build. Mater.* **2019**, *218*, 543−555.
(50) Qoku, E.; Bier, T. A.; Westphal, T. Phase assemblage in ettringite-forming cement pastes: A X-ray diffraction and thermal analysis characterization. *J. Build. Eng.* **2017**, *12*, 37−50.

https://doi.org/10.1021/acsomega.3c09804
ACS Omega 2024, 9, 10799−10811

(51) Trauchessec, R.; Mechling, J. M.; Lecomte, A.; et al. Hydration of ordinary Portland cement and calcium sulfoaluminate cement blends. *Cem. Concr. Compos.* **2015**, *56*, 106−114.

https://doi.org/10.1021/acsomega.3c09804
ACS Omega 2024, 9, 10799−10811